Investigation of Stationary-Crossflow-Instability Induced Transition with Temperature-Sensitive Paint Method

Jonathan Lemarechal[1]*, Marco Costantini[1], Christian Klein[1], Markus J Kloker[2], Werner Würz[2], Holger BE Kurz[2], Sven Schaber[3]

[1] German Aerospace Center (DLR), Institute of Aerodynamics and Flow Technology, Göttingen, Germany

[2] University of Stuttgart, Institute of Aerodynamics and Gas Dynamics, Stuttgart, Germany

[3] Airbus Operations, Bremen, Germany

*jonathan.lemarechal@dlr.de

Abstract

The Temperature-Sensitive Paint (TSP) method is used for surface-based flow visualizations on a swept-wing wind-tunnel model with a generic natural laminar-flow profile. Within the investigated parameter range the stationary crossflow instability is the dominating instability mechanism. Based on the TSP results the location of the laminar-turbulent transition and the most amplified wavenumber of the stationary crossflow instability are derived. The test is performed with three different conditions of the leading-edge surface: highly polished, unpolished, and highly polished with discrete roughness elements applied. With the discrete roughness elements, i.e. cylindrical elements with micron-sized height, the transition could be delayed successfully for certain conditions. Local low-frequency movement of the beginning of turbulent wedges was detected for some data points with an unpolished leading edge. The Temperature-Sensitive Paint method has proven to have sufficient spatial resolution and temperature sensitivity to resolve skin friction variations to detect the footprint of stationary crossflow vortices even inside of turbulent wedges.

1 Introduction

A swept wing inherently develops a three-dimensional boundary layer, which is prone to stationary crossflow (CF) instability. The receptivity to surface roughness is the most important mechanism for feeding the stationary CF instability in a low turbulence environment, i.e. even smallest surface roughness causes significant initial amplitudes for CF instability to develop in a three-dimensional boundary layer. Details on CF instability are given by Bippes (1999), and on CF receptivity by Kurz and Kloker (2014). The latter mechanism can be used to delay laminar to turbulent transition by applying discrete roughness elements (DRE) with the correct size and spacing at the leading edge, as described by Radetzsky et al. (1999). The DRE trigger a higher-wavenumber mode, which grows initially stronger than the natural mode, typically growing strongest on the long run. This delays the transition by nonlinear suppression of the natural mode. Generally, the method has been termed Upstream Flow Deformation (UFD) by Wassermann and Kloker (2002).

The boundary-layer transition and the CF vortices´ footprints are experimentally studied in this work with the Temperature-Sensitive Paint (TSP) method, which is a non-intrusive thermographic measurement technique with high spatial resolution (Fey and Egami 2007). In the present experiment three different conditions of the leading-edge surface were examined: highly polished, highly polished with spray-coated DRE, and unpolished.

2 Experimental Setup

The presented experiment was conducted in the Laminar Wind Tunnel of the Institute of Aerodynamics and Gas Dynamics, which has a very low turbulence level of $Tu = 0.02\%$ at 30 m/s and is thus well suited for the investigation of stationary CF instabilities. The generic wind tunnel model was especially designed to achieve a quasi-infinite swept-wing flow in the middle third of the model. The model is untapered with a sweep angle of $\varphi = 25°$, a chord of $c = 1$ m, and a span of 0.73 m. It was completely manufactured from aluminum by NC-milling. The cross section, pressure distribution, and stability diagram are shown in figure 1. The pressure distribution provides a favorable pressure gradient up to $x/c = 0.5$ (figure 1a), which enables the stationary crossflow instability to grow (figure 1b). The naturally most amplified dimensionless stationary-crossflow wavenumber ($\gamma = 2\pi/\lambda \cdot c \cdot \cos(\varphi) \approx 1400$) for the wind tunnel tests is similar to the most excited ones reported by Schrauf et al. (1998) from measurements in flight.

During the tests the pressure distribution was measured for stability calculations and the transition location was measured to assess the leading-edge surface influence. Transition measurements were performed with the TSP method. Details about TSP measurements are given by Liu and Sullivan (2005) and further details concerning the necessity of a heat flux between model and flow for thermographic measurement techniques in low-speed tests are given by Fey and Egami (2007). For the present investigation the heat flux was realized by continuously blowing hot air through the hollow wind tunnel model.

On the pressure side of the model two pockets, which are separated by a metallic strip containing the pressure taps, are coated with the TSP explained in detail by Ondrus et al. (2015). The TSP and metallic surfaces were polished to a mirror-like finish ($R_z = 0.33$ μm) and the interfaces between TSP and metallic were treated to a high quality, i.e. gaps narrower than 200 μm with an average depth of 5 μm. The TSP technique was applied in the intensity based method: Two LEDs (HARDsoft® Illuminator UV) were used to excite the TSP and two types of black-and-white camera, i.e. a scientific 14-bit CCD camera (pco.4000) and a 12-bit CMOS camera (PHOTRON FASTCAM SA1), were used to record the emitted light. The CCD camera was used to record the entire model with 0.5 Hz acquisition frequency and a spatial resolution of 0.2 mm/px; the CMOS camera was used for time-resolved TSP visualization of a detail of the model with 1 kHz acquisition frequency and a spatial resolution of 0.3 mm/px.
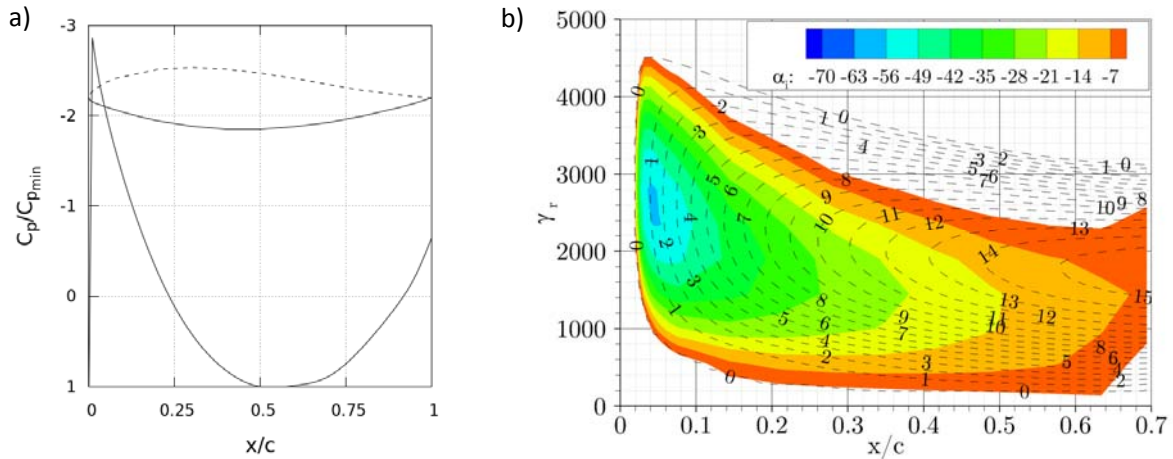

Figure 1: Pressure distribution c_p of the pressure (lower) side and the model cross section a). The stability diagram b) for $Re_c = 5.00 \cdot 10^6$ at an angle of attack $\alpha = 6.0°$, stationary crossflow modes ($\omega_r = 0$). the spatial amplification rate α_i (colored contours), and the N-factor (dashed lines).

The stability properties of the boundary layer are determined in two steps: First, a boundary layer integration is performed using the measured c_p distribution. Second, growth rates for stationary crossflow modes are computed with a compressible spatial linear-stability solver with one-dimensional eigenfunctions, assuming locally parallel flow and neglecting curvature effects; further details are given by Kurz and Kloker (2014).

3 Results

The Reynolds-number range of the investigations is $Re_c = 3.77 \cdot 10^6 - 5.00 \cdot 10^6$ and the angle of attack was set to $\alpha = 6°$. An example of a TSP result is given in figure 2. Darker areas correspond to higher heat transfer, which can be caused by turbulent flow or stationary CF vortices, i.e. parallel lines leading up to the turbulent flow. The brighter areas correspond to lower heat transfer, i.e. laminar flow. The typical saw-tooth pattern of CF-induced transition is visible in figures 2 and 3a). The result in figure 2) was acquired with an unpolished leading edge. The visible footprint of the CF vortices varies from vortex to vortex, which is interpreted as a variation in vortex strength. An increase of the vortex strength along its axis is however barely visible. This leads to the conclusion that the CF vortices are only visible in the nonlinear growth regime, when the growth saturates. As expected, strong vortices, i.e. with especially dark footprint, lead to the onset of the turbulent wedges. Note also that the vortex next to the one leading to the wedges is also stronger than the surrounding ones. The early onset of transition is probably caused by a particularly large event in the surface texture at the leading edge region, which provides locally a large initial amplitude for the CF instability. The structure inside of the turbulent wedge shows a continuation of the vortex footprint, i.e. the gap between the two strong vortices leading up to the tip of the wedge is continued in the turbulent area. This behavior was also described by Dagenhart et al. (1989) in experiments with sublimating chemicals.
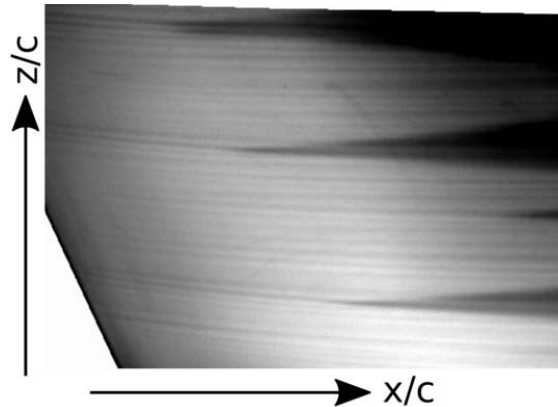

Figure 2: Detail of the TSP visualization with excellent visibility of the footprint of the stationary crossflow vortices and the laminar-turbulent transition. The vortex footprint remains visible in the turbulent area.

Besides the surface temperature variation caused by flow structures, also the distribution of the heat capacity of the model due to spars and ribs, is visible as brighter horizontal and vertical lines, e.g. at $x/c = 0.32$ in figure 3c). This inhomogenous distribution of the heat capacity causes another drawback: a large temperature difference between model surface and flow is needed to achieve sufficient contrast for the flow structures. The average overheating ratio throughout the test was $T_m/T_f = 1.07$. Dovgal et al. (1990) found in their experiments with a heated model leading edge ($T_m/T_f \approx 1.21$) that the boundary layer is destabilized and transition occurs earlier. This behavior was not found in the present investigations and could be proofed by variation of the heating power was. However, the development of electrical heating, e.g. carbon nanotubes as introduced by Klein et al. (2014), and wind tunnel models with homogenous heat capacity distribution is vital for improving the quality of TSP results.

The TSP method was also used for investigating spray-coated DRE (height $h = 11.8\,\mu m$, diameter $\emptyset = 0.88$ mm, spanwise spacing $\Delta z = 2$ mm at $x/c = 0.03$) at various chord Reynolds numbers and at fixed $\alpha = 6°$. A detail of the TSP result, which is directly comparing the transition location of the clean configuration and the DRE-delayed transition, is shown in figure 3a and 3c, respectively. Two prominent differences are visible: delay of the transition location and a stronger footprint of the stationary CF vortices with a larger spacing and earlier beginning with DRE, cf. figure 3c.

From the TSP data of figure 3a and 3c the wavenumber of the stationary CF vortex footprints was calculated by Fourier analysis, see figure 3b and 3d. Starting with the clean case (figure 3a) the visualization shows hardly any visible structures upstream of $x/c = 0.3$ but the wavenumber spectrum in figure 3b shows several peaks including the expected wavenumber of $\gamma = 1400$. Further downstream the transition starts in CF vortices with a distance of $\gamma \approx 500$ (figure 3a at $x/c = 0.35$), which is smaller than the predicted naturally most amplified wavenumber. The transition is located at $x/c \approx 0.41 \pm 0.02$.
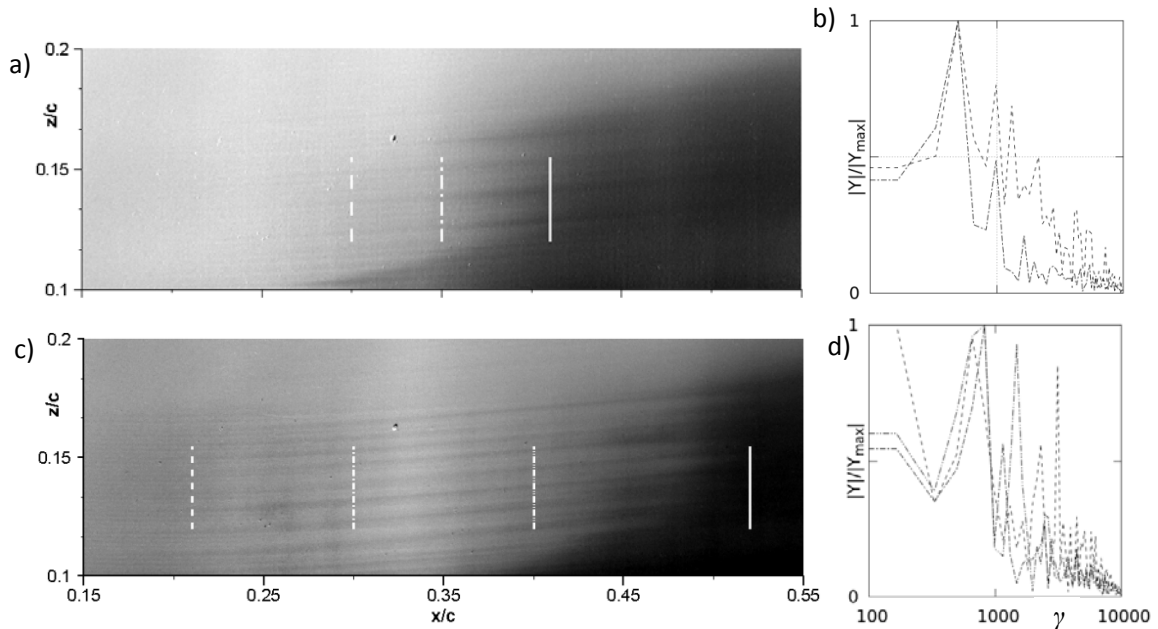

Figure 3: TSP visualization for $Re_c = 5.0 \cdot 10^6$ and $\alpha = 6.0°$ of polished surface a) in comparison to the polished surface with spray coated DRE c). b) and d) show the amplitude spectrum of the wavenumber derived from the line cuts indicated with the same line style in a) and c), respectively. The solid lines in a) and c) mark the transition location.

When the UFD mode ($\gamma = 2850$) is triggered by the DRE this is visible in the wavenumber distribution (figure 3d) and also in the visualization (figure 3c), where an evenly spaced vortex footprint is already visible at $x/c \approx 0.21$. Additionally to the triggered wavenumber mode, a low wavenumber mode ($\gamma \approx 850$) appears. Note that further downstream this wavenumber remains of significant impact on the footprint. Closer to the transition location the naturally most amplified wavenumber ($\gamma = 1400$) appears. The UFD mode delays transition to $x/c \approx 0.52 \pm 0.02$ for $Re_c = 5.0 \cdot 10^6$.

The test showed a linear variation of the transition location with increasing Reynolds number. Transition delay sets in for $Re_c \geq 4.8 \cdot 10^6$ (figure 4a), where the DRE mode reaches sufficiently high N-factors (and thus amplitudes) while still remaining below the critical N-factor, see the dashed line in figure 4b. When transition is successfully delayed the introduced UFD mode is detectable in the TSP result at $x/c \approx 0.21$ (figure 3c) but the mode leading to transition has a wavenumber of $\gamma \approx 850$, which was not observed in the clean case. At $Re_c < 4.7 \cdot 10^6$ the transition of the clean configuration is so far aft, that introducing the UFD-mode causes premature transition. Although the N-factor of the UFD mode is relatively small under these conditions, a nonlinear interaction between the modes is likely to cause the premature transition.

In comparison with the flight experiments of Saric et al. (2015), which were performed at similar chord Reynolds numbers, the achievable transition delay was larger in the present experiment.

During the experiments an unexpected phenomenon was observed: a low-frequency variation of the turbulent wedge onset location of some CF vortices. This behavior was observed for configurations with a non-polished leading edge. To further investigate this unsteadiness, a data point was repeated with the
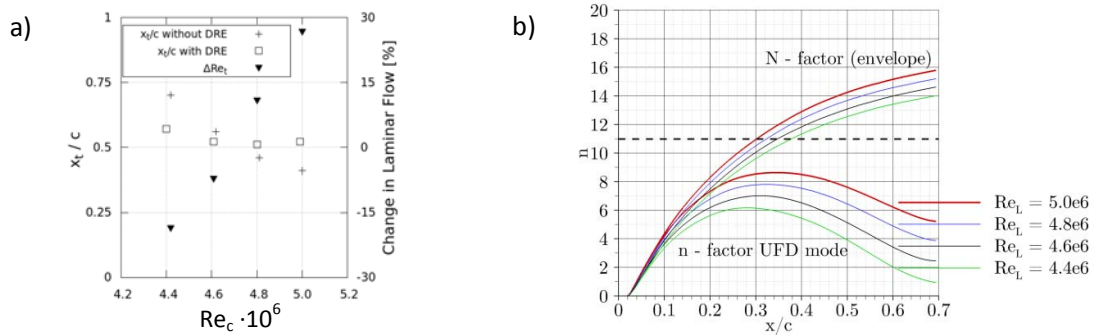
Figure 4: Transition variation by DRE for different chord Reynolds numbers at α = 6.0° a), and the N-factor diagram of the envelope and UFD mode b).
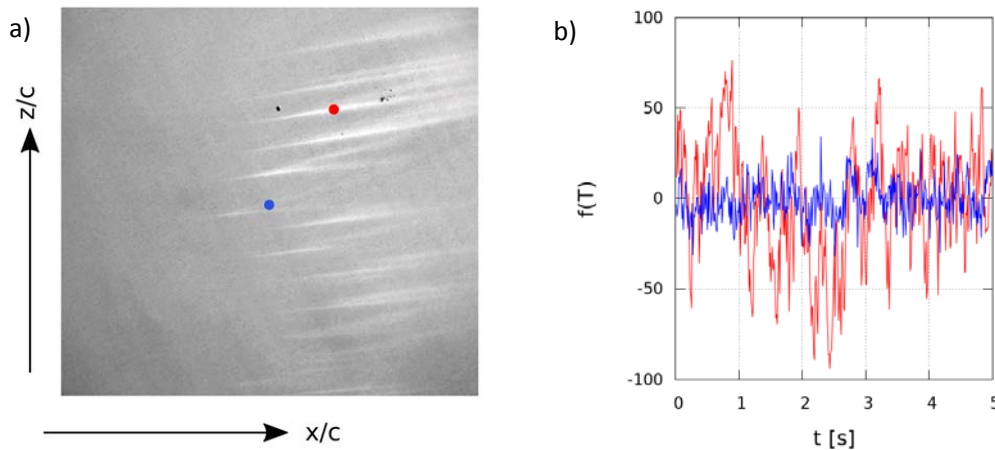

Figure 5: RMS of a time-resolved acquisition with a high-speed camera a). Time-series of the intensity ratio (f(T)) of a stationary crossflow vortex with unsteady (red) and steady (blue) transition onset, respectively, b).

high-speed camera and the root mean square (RMS) of each pixel was calculated for each pixel, see figure 5a. In the RMS result brighter areas indicate regions of larger variations.

The RMS results indicate that the onset of the turbulent flow, which is forming the saw tooth pattern, varies significantly during the measurement time. Also the turbulent wedges have significantly different RMS values. A steady wedge (indicated in blue) starts more upstream than the surrounding more unsteady wedges. The increased RMS is caused by the back and forth motion in flow direction of the onset of the wedge. From the time-resolved measurement the variation of the intensity ratio over time is shown for two turbulent wedges, one with steady and one with unsteady behavior in figure 5b. A low-frequency movement without any dominating frequency along the vortex axis is visible for the unsteady wedge. The onset of the wedge marked with the red symbol moves 44 mm ($Δx/c = 0.044$) in flow direction during the measurement time. The fact that the movement of the wedges seems to be independent for each wedge indicates that a local mechanisms causes this variation.

4 Conclusion

The Temperature-Sensitive Paint (TSP) method was used to study laminar-turbulent transition, which was induced by stationary crossflow instability. Besides the transition location the footprint of the stationary crossflow vortices was visualized. From the experimental data, the wavenumber was derived and compared to linear stability calculations. Good agreement between the predicted wave numbers from the

linear stability calculations and the TSP results was assessed. Furthermore, a local variation of transition location was observed for the case of an unpolished leading-edge surface. In the case of a highly-polished leading-edge surface transition was successfully delayed for the two highest Reynolds numbers tested by applying discrete roughness elements. To further increase TSP capabilities the development of homogenous heating possibilities, e.g. CNT and carbon fiber, is envisaged. Controlled electrical heating and a model with a homogenous heat capacity distribution would allow comparing vortex strengths from data point to data point.

Acknowledgements

References

Bippes H (1999) Basic experiments on transition in three-dimensional boundary layers dominated by crossflow instability. *Progress in Aerospace Sciences* 35:363-412

Dagenhart JR, Saric WS, Mousseux MC, and Stack JP(1989) Crossflow-vortex instability and transition on a 45 deg swept wing. AIAA-89-1892

Dovgal AV, Levchenko VY, and Timofeev VA (1990) Boundary Layer Control by a Local Heating of the Wall. In: Arnal D, Michel R (eds.) *Laminar-Turbulent Transition*. International Union of Theoretical and Applied Mechanics (IUTAM). Springer, Berlin, Heidelberg

Fey U and Egami Y (2007) Transition-Detection by Temperature-Sensitive Paint. In: Tropea C, Yarin AL, Foss JF (eds) Springer Handbook of Experimental Fluid Mechanics. Springer, Berlin

Klein C, Henne U, Sachs WE, Beifuß U, Ondrus V, Bruse M, Lesjak R, and Löhr M (2014) Application of Carbon Nanotubes (CNT) and Temperature-Sensitive Paint (TSP) for Detection of Boundary Layer Transition. AIAA 2014-1482

Kurz HBE andx Kloker MJ (2014) Receptivity of a sept-wing boundary layer to micron-sized discrete roughness elements. *Journal of Fluid Mechanics* 755:62-82

Liu T and Sullivan JP (2005) Pressure and Temperature Sensitive Paints. ISBN 3-540-22241-3

Ondrus V, Meier RJ, Klein C, Henne U, Schäferling M, and Beifuß U (2015) Europium 1,3-di(thienyl)propane-1,3-diones with Outstanding Properties for Temperature Sensing. *Sensors and Actuators A: Physical* 233:434-441.

Radetzsky RH, Reibert MS, and Saric WS (1999) Effect of Isolated Micron-Sized Roughness on Transition in Swept-Wing Flows. *AIAA Journal* 37:1370-1377

Saric WS, West DE, Tufts MW, and Reed HL (2015) Flight Test Experiments on Discrete Roughness Element Technology for Laminar Flow Control. AIAA 2015-0539

Schrauf G, Perraud J, Vitiello D, and Lam F (1998) Comparison of Boundary-Layer Transition Predictions Using Flight Test Data. *Journal of Aircraft* 35:891-897

Wassermann P and Kloker MJ (2002) Mechanisms and passive control of crossflow-vortex-induced transition in a three-dimensional boundary layer. *Journal of Fluid Mechanics* 456:49-84